A 12%-Efficient Upgraded Metallurgical Grade Silicon–Organic Heterojunction Solar Cell Achieved by a Self-Purifying Process

Jie Zhang,[†] Tao Song,[†] Xinlei Shen,[‡] Xuegong Yu,[‡] Shuit-Tong Lee,[†] and Baoquan Sun*,[†]

[†]Institute of Functional Nano and Soft Materials (FUNSOM), Soochow University, Suzhou 215123, Jiangsu, China and [‡]State Key Laboratory of Silicon Materials and Department of Materials Science and Engineering, Zhejiang University, Hangzhou 310027, China

ABSTRACT Low-quality silicon such as upgraded metallurgical-grade (UMG) silicon promises to reduce the material requirements for high-performance cost-effective photovoltaics. So far, however, UMG silicon currently exhibits the short diffusion length and serious charge recombination associated with high impurity levels, which hinders the performance of solar cells. Here, we used a metal-assisted chemical etching (MACE) method to partially upgrade the UMG silicon surface. The silicon was etched into a nanostructured one by the MACE process, associated with removing impurities on the surface. Meanwhile, nanostructured forms of UMG silicon can benefit improved light harvesting with thin substrates, which can relax the requirement of material purity for high photovoltaic performance. In order to suppress the large surface recombination due to increased surface area of nanostructured UMG silicon, a post chemical treatment was used to decrease the surface area. A solution-processed conjugated polymer of poly(3,4-ethylenedioxythiophene):poly(styrenesulfonate) (PEDOT:PSS) was deposited on UMG silicon at low temperature (<150 °C) to form a heterojunction to avoid any impurity diffusion in the silicon substrate. By optimizing the thickness of silicon and suppressing the charge recombination at the interface between thin UMG silicon/PEDOT:PSS, we are able to achieve 12.0%-efficient organic–inorganic hybrid solar cells, which are higher than analogous UMG silicon devices. We show that the modified UMG silicon surface can increase the minority carrier lifetime because of reduced impurity and surface area. Our results suggest a design rule for an efficient silicon solar cell with low-quality silicon absorbers.

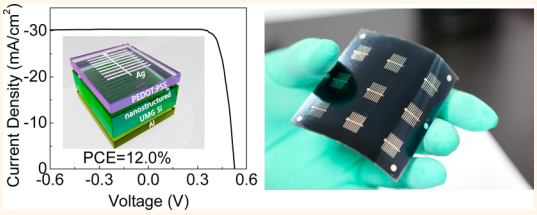

KEYWORDS: upgraded metallurgical-grade silicon · surface modification · charge recombination · organic–inorganic heterojunction · solar cell

Considerable efforts have been expended in the past decades on silicon solar cell fabrication technologies to cope with people's ever-growing electric power requirement. The main limitation for silicon solar cells is still imposed by the high cost due to complicated fabrication processes and expensive materials, especially the energy-consuming silicon purification process.[1−3] Usually traditional commercial crystal solar cells are fabricated from high-quality silicon materials,[4] for example, solar-grade (SG) silicon to achieve favorable device performance, where SG silicon displays a relatively long minority carrier diffusion length.[5] Around 30% of the cost of Si-based solar cell comes from silicon wafers due to the complexities of the purifying process.[6] Simplifying the fabrication procedures and using low-quality silicon is a conceptually straightforward route to reduce the cost of the resulting silicon solar module.

Upgraded metallurgical-grade (UMG) silicon is generally prepared by a relative simple chemical refining process, which is almost ∼5−10 times cheaper than SG silicon. Unfortunately, the power conversion efficiency (PCE) of a solar cell based on UMG silicon is relatively low.[7] The major disadvantage of UMG silicon is ascribed to the high impurity level, leading to a short minority carrier diffusion length accompanied by serious charge recombination. There are two main strategies to use UMG silicon for efficient solar cells: reducing the thickness of the silicon layer[8,9] or using nanostructured silicon to build up radial junctions.[10,11]

* Address correspondence to bqsun@suda.edu.cn.

Received for review August 1, 2014 and accepted November 3, 2014.

Published online November 03, 2014
10.1021/nn504279d

A thin silicon layer (<20 μm) had been used to fabricate solar cells with a PCE up to 8%, where silver nanoparticles atop silicon nanopillars were utilized to enhance light absorption.[8] More recently, ultrathin (~12 μm) UMG silicon solar cells yielded an efficiency of ~11%,[9] which was achieved by multiple plasmonic layers precisely positioned on top of the cell to enhance light absorption. This method is very promising to achieve high PCE UMG silicon solar cells due to simple device structure. However, further work is necessary to develop solar cells utilizing thin silicon films due to silicon's poor absorption. Nanostructured silicon displays its potential to significantly reduce the usage of active materials, relaxing the requirement of silicon purity. Nanostructured silicon technologies start from a UMG silicon wafer to build up a radial junction, where the light absorption direction and charge transport direction are orthogonal. This strategy can overcome the disadvantage of short carrier diffusion length of UMG silicon,[9] achieving a PCE up to 8.7%. These technologies are attractive; however, the efficiency is still much lower in comparison with the high-quality silicon device. Recently, Wehrspohn and his colleagues reported that "dirty" silicon as a starting material can be used to upgrade its purity to solar grade *via* a metal-assisted chemical etching (MACE) process.[12] Metal impurities can be removed upon exposing the silicon surface to an acidic etchant solution. However, the advantage of surface-purified silicon cannot be maintained for high-performance solar cells because the inner side metal purity can diffuse into the surface again in the traditional high-temperature doping process.[13]

Here, we developed a facile and low-cost method for efficient UMG silicon solar cells at a low temperature. The impurity in the UMG silicon surface was partly removed when the surface was etched into nanostructured form by the MACE process. In addition, nanostructured silicon can achieve efficient light harvesting with a thin substrate, which can relax the high purity requirement for a long minority carrier distance. In order to suppress the serious surface charge recombination due to the large silicon surface area, a chemical post-treatment was developed to minimize the surface area while maintaining good light-harvesting capability. A conductive polymer of poly(3,4-ethylenedioxythiophene):poly(styrenesulfonate) (PEDOT:PSS) was deposited onto nanostructured silicon to form an organic–inorganic heterojunction with a low-temperature process. By controlling the junction quality, an optimum efficiency of 12.0% has been achieved for the UMG-based silicon solar cell, which is higher than analogous UMG silicon devices.

RESULTS AND DISCUSSION

It is known that low-quality silicon shows a reduced minority diffusion length.[14] A thin silicon film can overcome the disadvantage of a short minority diffusion length. However, if silicon thickness is larger than the minority carrier diffusion length, the electrodes would not collect charge carriers effectively, thus leading to the reduction of current density. In order to verify this point, UMG silicon is etched into various thicknesses to collect charge carriers efficiently.[15] With this technology, a wafer-scale-size UMG silicon substrate can be obtained with reduced thickness to compensate for the drawback of the short minority diffusion length, while it is also associated with weak optical absorption of silicon for photons. Figure S1 shows the cross-sectional scanning electron microscope (SEM) images of the UMG silicon substrates with different thicknesses. Unfortunately, light can penetrate the silicon substrate in longer wavelengths as the silicon substrate becomes thinner (Figure S2). Thus, although thin UMG silicon can compensate for the disadvantage of its short diffusion length, it is also accompanied by a reduction in light harvesting, resulting in low photogenerated current. The devices based on PEDOT:PSS and planar silicon of different thicknesses are fabricated to investigate the thickness of the UMG silicon *versus* their respective photovoltaic performances, as shown in Figure S2. The electrical output characteristics are summarized in Table S1. The device based on UMG planar silicon with a thickness of ~95 μm yields a relatively high PCE; therefore, the optimized thickness of ~95 μm is used to balance the light harvesting and charge collection.

Previously, in order to enhance light harvesting, either nanoparticle[8] or nanopillar[16] arrays can be utilized for enhancing optical absorption in silicon solar cells. Here, nanostructured silicon is fabricated to increase light absorption. Meanwhile, the impurities can partly be removed in the nanostructured silicon fabrication process. Nanostructured silicon was prepared by the MACE method.[16] In addition, the silicon surface is modified by anisotropic tetramethylammonium hydroxide (TMAH)[17] to decrease the silicon surface area. Figure 1a–c display diagrammatic sketches of the nanostructured silicon formation process prepared with the MACE method. The silver ions near the surface of the silicon substrate catch electrons from silicon and are deposited on the silicon surface to form silver clusters acting as a cathode. In other words, great numbers of self-assembled electrochemical cells are formed on the surface of the silicon substrate. Meanwhile, silicon loses electrons and is oxidized into SiO_2. Then SiO_2 is dissolved simultaneously in HF solution.[18] The redox reaction and SiO_2 dissolvation take place only near the silver clusters. Metal ion impurity particles are etched away as they are exposed to an etching agent.[12,19] In a sense, this kind of nanostructured UMG silicon is purified as the metal ion impurities are eliminated.

Although there are several possible factors that can result in the phenomenon of removing metal

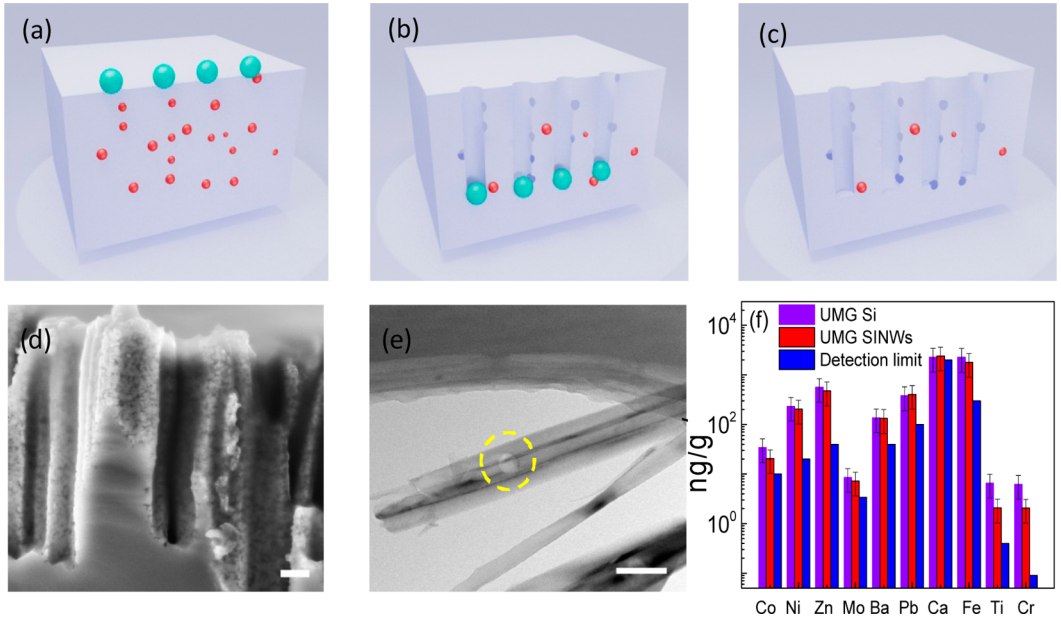

Figure 1. (a–c) Diagrammatic sketches of the nanostructured UMG silicon formation process. The red spots in the sketches represent the impurity clusters in UMG silicon, and the aquamarine spots represent silver particles. (d) Cross-section SEM images of nanostructured silicon fabricated from UMG silicon. The scale bar is 100 nm. (e) TEM images of silicon nanowires scratched from a nanostructured UMG silicon substrate. The scale bar is 100 nm. (f) Impurity concentrations of thin UMG silicon before and after the MACE process measured by ICP-MS, respectively.

impurities,[20−22] we believe that metal impurities dissolving upon exposure to the acidic etchant solution is the dominant factor. It is known that hydrogen peroxide (H_2O_2) may lead to a porous structure if it is added in the etching solution, so the use of H_2O_2 is avoided in the MACE process. It can be observed from Figure S3 that SG silicon nanostructures with similar doping levels etched under the same etching conditions have no porous structure on the SiNWs' wall side, suggesting that the porous structure in UMG silicon is not caused by H_2O_2 but by metal impurities dissolving. Figure 1d shows SEM images of nanostructured UMG silicon. On the wall of nanostructured silicon, there are many pits with a diameter of around 20−30 nm, which are ascribed to the increased etching velocity due to the presence of the impurities in UMG silicon. The impurities are removed simultaneously after the MACE process. For nanostructured silicon etched from SG silicon, such pits are absent, as shown in Figure S3d, indicating that these pits are formed only when large impurity particles are exposed to the etching solution. This phenomenon is also confirmed by transmission electron microscope (TEM) images in Figure 1e. There are holes on silicon nanowires, revealing that this impurity spot is etched away. To further verify that surface purification has occurred, inductively coupled plasma mass spectrometry (ICP-MS) is used to monitor the metal ion concentration variation before and after the MACE process. In Figure 1f, several metal elements in UMG silicon are listed before and after the MACE process. It is found that most element concentrations are decreased, such as Co, Fe, Zn, Ni, and Mo, which is consistent with the previous observation.[12] The results indicate that the quality of silicon was upgraded on the surface.

Recently, the emergence of hybrid organic−silicon solar cells has promised an alternative path to reduce cost by adopting low-temperature, soluble processes of conjugated polymers to form heterojunctions with silicon.[23−35] Interface engineering currently plays a key role in the performance of hybrid organic−silicon heterojunction solar cells.[27] Here, great efforts are made to improve the interface quality of the conjugated polymer/Si heterojunction. PEDOT:PSS is used for organic contact due to its high conductivity and easy processing. For further elucidating the surface modification effects on the heterojunction quality of silicon/PEDOT:PSS, Figure 2 is plotted to illustrate the energy band alignment diagram of the junction based on (a) planar UMG silicon, (b) nanostructured UMG silicon, and (c) nanostructured UMG silicon treated with TMAH. Here, we assume that PEDOT:PSS/n-Si is a Shottcky junction.[36] For UMG silicon (Figure 2a), the Shockley−Read−Hall (SRH) recombination *via* the metal-induced deep electronic states dominates the charge recombination process due to its high impurity levels.[14] In the purification process by the MACE method, the surface silicon quality was upgraded; the SRH recombination near the surface might be suppressed due to the decreased impurity concentration level, as shown in Figure 2b. Unfortunately, the large nanostructured surface may still lead to severe recombination.[17] In order to reducing the surface area, a subsequent TMAH etching process is introduced to

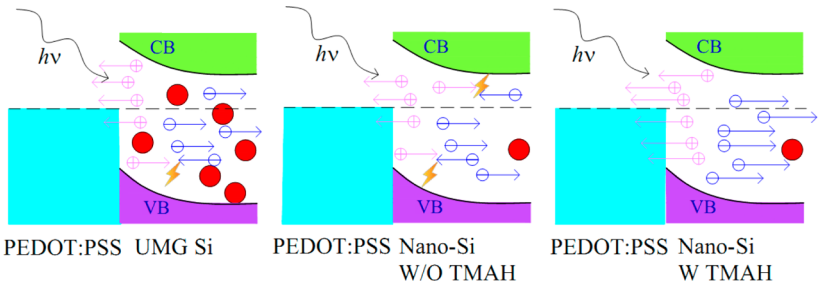

Figure 2. Energy band alignment diagram of (a) PEDOT:PSS/planar UMG silicon, (b) PEDOT:PSS/nanostructured UMG silicon, and (c) PEDOT:PSS/nanostructured UMG silicon treated with TMAH etching solution. The red spots represent metal ion impurities. The flashing spots stand for charge recombination.

control the final surface morphology to suppress charge recombination.[17] In combination with the surface purification and reducing surface area, charge recombination can be dramatically suppressed at the junction, as shown in Figure 2c. Figure S3a and b compare the cross-section images of UMG silicon without any TMAH etching and with a 15 s TMAH modification. The unmodified UMG silicon displays many pores, which are partly caused by releasing impurity clusters. The TMAH modification decreases the nanostructured front surface area by "polishing" and widening the distance of wires to suppress their areal density. Meanwhile, according to the reflection and absorption of the three kinds of substrates shown in Figure S4, the TMAH etching process can still preserve the light-harvesting capability. In addition, the modified UMG silicon nanostructure favors PEDOT:PSS to form a continuous film due to increasing the adjacent distances between the silicon wires. As shown in Figure S3c, PEDOT:PSS forms a compact and continuous layer on nanostructured UMG silicon, which ensures an efficient organic–inorganic coupling interaction.

In order to verify the surface recombination suppression after treatment, minority carrier lifetime mapping measurements based on a microwave photoconductance decay technique for the silicon substrate with different surface treatments were carried out. In a silicon solar cell, the effective minority carrier lifetime is determined by both bulk recombination and surface recombination, which can be expressed by eq 1:[37]

$$\frac{1}{\tau_{meas}} = \frac{1}{\tau_{bulk}} + \frac{2S}{W} \quad (1)$$

Here τ_{meas} is the measured effective minority carrier lifetime, τ_{bulk} is the bulk recombination lifetime, S is the surface recombination velocity, and W is the silicon thickness. Note that the minority carrier lifetime of the bulk material is constant. The variation of measured minority carrier lifetime of silicon should originate from surface recombination. Different samples were prepared with various surface morphologies: (a) nanostructured UMG silicon (Nano-Si); (b) nanostructured UMG silicon coated with PEDOT:PSS; (c) nanostructured UMG silicon treated with TMAH and spin coated with PEDOT:PSS. These exhibit average minority carrier lifetimes of 2.9, 4.7, and 5.2 μs, respectively. The minority carrier lifetime mapping measurements of the different samples are illustrated in Figure 3. The bare nanostructured UMG silicon displays large surface areas, accompanied by a great number of defects. These defects lead to serious charge recombination at the surface. When PEDOT:PSS was deposited onto the nanostructured UMG silicon, the minority carrier lifetime increases from 2.9 μs to 4.7 μs. The enhancement of the carrier lifetime originates from the variation of energy band bending near the Si/PEDOT:PSS interface. A strong inversion layer usually takes place in a Si/PEDOT:PSS hybrid solar cell. The formation of a strong inversion layer definitely decreases the concentration of minority carriers at the Si/PEDOT:PSS interface, therefore correspondingly reducing the carrier recombination probability. Meanwhile, the PEDOT:PSS film can passiviate the dangling bond on the surface of nanostructured UMG silicon, which also suppresses the carrier recombination at the interface. After nanostructured UMG silicon is treated with TMAH, the surface area decreases, accompanied by reduced charge recombination. When nanostructured UMG silicon is processed by combining the MACE method and THAH treatment, the effective carrier lifetime is dramatically improved, as a result of improving the surface passivation. The microwave photoconductance decay measurements confirm that the combination of surface purification and morphologies can enhance minority carrier lifetime, associated with reduced charge recombination.

Solar cells based on UMG silicon with different surface morphologies are fabricated to explore their photovoltaic performance. The device structure is illustrated in Figure 4d. As mentioned previously, the optimum UMG silicon thickness is ~90 μm to balance the light-harvesting and charge collection. Figure 4 shows the current–voltage (J–V) curve of the UMG silicon hybrid solar cell with different surface morphologies. The electrical output characteristics are summarized in Table 1. The best device based on nanostructured UMG silicon with TMAH treatment displays an open-circuit voltage (V_{OC}) of 0.523 V, a short-circuit current (J_{SC}) of 30.9 mA/cm^2, and a fill factor (FF) of

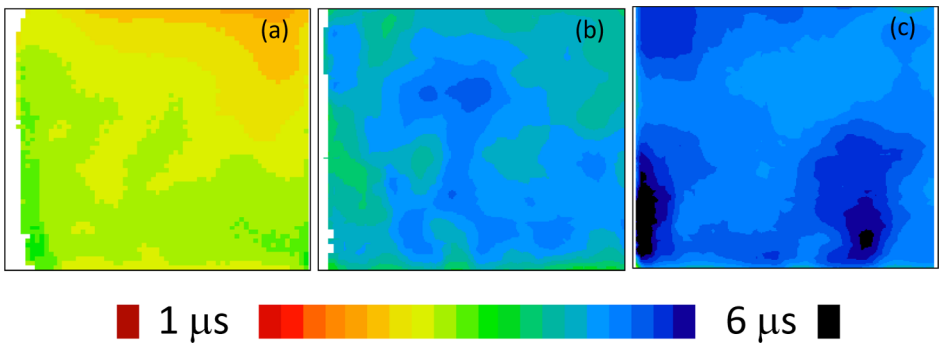

Figure 3. Minority carrier lifetime mapping for the different samples: (a) bare nanostructured UMG silicon; (b) nanostructured UMG silicon/PEDOT:PSS; (c) nanostructured UMG silicon (treated with TMAH)/PEDOT:PSS.

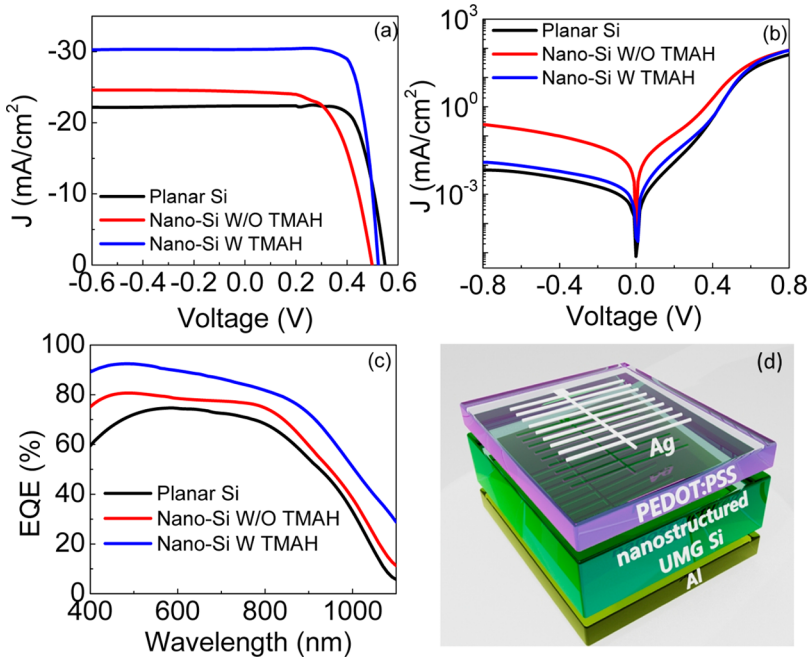

Figure 4. Electric output characteristics of the Si/PEDOT:PSS devices with different surface modification. (a) *J*–*V* curves under illumination at 100 mW/cm^2, (b) *J*–*V* curves under dark, and (c) EQE spectra. (d) Device structure of the nanostructured UMG silicon/PEDOT:PSS hybrid solar cell.

TABLE 1. Electric Output Characteristics of the Devices Based on Nanostructured UMG Silicon with Different Surface Modification: (1) Planar UMG Silicon; (2) Nanostructured UMG Silicon; (3) Nanostructured UMG Silicon Treated with TMAH

device	V_{OC} (V)	J_{SC} (mA/cm^2)	FF	PCE (%)
planar-Si	**0.550**[b]	**22.3**	**0.724**	**8.88**
	0.551 (±0.001)[a]	21.9 (±0.4)	0.718 (±0.006)	8.66 (±0.22)
Nano-Si	**0.499**	**24.4**	**0.603**	**7.34**
	0.495 (±0.004)	24.4 (±0.1)	0.597 (±0.006)	7.21 (±0.13)
Nano-Si with TMAH	**0.523**	**30.9**	**0.745**	**12.0**
	0.524 (±0.001)	30.7 (±0.2)	0.738 (±0.007)	11.9 (±0.10)

[a] Data and statistics are based on 10 devices for each type. [b] Numbers in bold are the maximum recorded values.

0.745, yielding a PCE of 12.0%. This PCE is dramatically enhanced in comparison with that of the planar UMG silicon solar cell (8.88%). It is also a record performance based on UMG silicon solar cells. On the contrary, the device based on nanostructured silicon without TMAH treatment exhibits a PCE of only 7.34% with an V_{OC} of 0.499 V, a J_{SC} of 24.4 mA/cm^2, and a FF of 0.603. This PCE is even lower than that of planar junction solar cells, which is ascribed to serious surface recombination.[27] The large surface area slightly enhanced the J_{SC} (24.4 mA/cm^2) for nanostructured silicon (without TMAH) *versus* the planar one due to reduced light reflection. Unfortunately, it also leads to poor FF and V_{OC} due to serious surface charge recombination. For more than 10 devices, the devices based on nanostructured UMG silicon with TMAH treatment give an average PCE of 11.9% for an optimized nanostructured UMG silicon device, as shown in Table 1. The J_{SC} of the hybrid devices based on different surface morphologies are consistent with the external quantum efficiency (EQE) spectra (Figure 4c). In addition, the leakage current is also suppressed when the nanostructured silicon is treated with TMAH, which indicates the

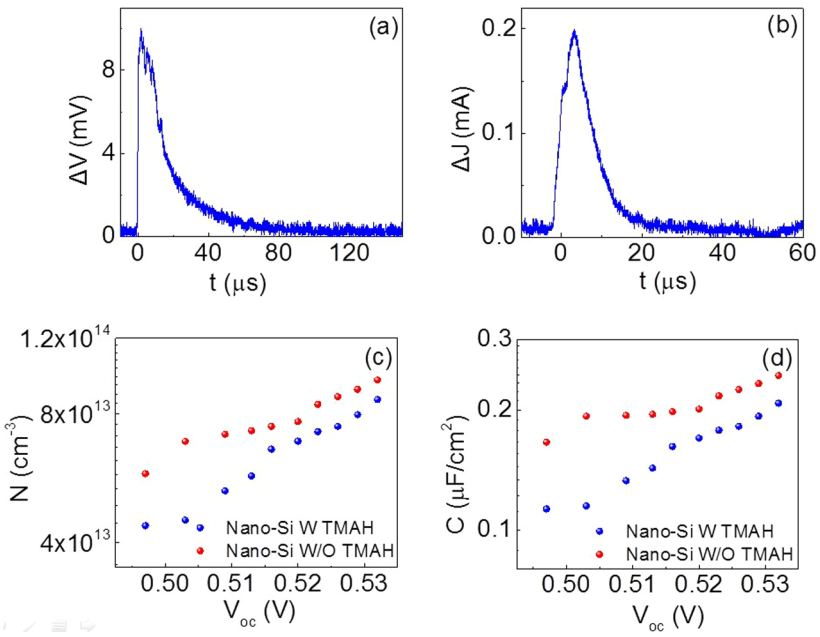

Figure 5. (a) Time-resolved transient photovoltage and (b) photocurrent decay measurement influenced by laser light pulse perturbation. (c) Charge carrier density *N vs* V_{OC} and (d) differential capacitance *C vs* V_{OC} for the devices based on nanostructured UMG silicon with/without TMAH treatment.

improved interface quality, as shown in Figure 4b. The post-TMAH treatment can decrease the surface area, dramatically suppressing the surface recombination, as discussed above.

A transient photovoltage decay measurement can provide a path to directly probe the recombination in photovoltaics.[10,38,39] Upon illumination at open circuit, a voltage is generated in the junction. Once the light is removed, charges should recombine, leading to a decay of the photovoltage. We performed transient photovoltage measurements in order to probe the charge recombination with different silicon surface morphologies. The V_{OC} perturbation transient induced by a pulsed incident power is measured at a simulating white light bias. Subsequently the change in charge density (ΔQ) is determined by integrating the short-circuit current transient induced by pulsed light. This charge corresponds to the stored charge in the organic−inorganic heterojunction by assuming charge generation is independent of an applied bias and recombination at short circuit is neglectable. The induced voltage change by the small charge addition through the short light perturbation defines the capacitance.[10,38] Time-resolved transient photovoltage/photocurrent decay measurements influenced by laser pulse perturbation are shown in Figure 5a and b, respectively. *C* and *N* are the capacitance and charge carrier concentration trapped by the interfacial defect states in the heterojunction with different values of V_{OC}, respectively. The detailed calculation method for *N* and *C* is described in the Supporting Information. The bias white light intensity is changed from 0.1 to 1 sun, and corresponding V_{OC} is changed from 0.497 to 0.532 V. Both *C* and *N* are illustrated in Figure 5, where *C* is plotted as a function of V_{OC} for devices based on nanostructured UMG silicon with or without TMAH treatment.

It can be observed in Figure 5 that transient photovoltage and photocurrent show desirable signal-to-noise resolution and are substantially easy to collect by a detector. ΔQ, which is the charge triggered by a laser pulse, is acquired by integrating transient photocurrent at short-circuit conditions with laser perturbation under different bias white light intensities. Therefore, *C* is calculated from ΔQ by dividing by ΔV_0, plotted in Figure 5. It is found that the devices based on nanostructured UMG silicon with or without TMAH treatment show different capacitances at the same voltage, which indicates the different charge extraction capability. The device based on UMG silicon with TMAH treatment gives a smaller capacitance than that of a device without TMAH treatment, which can be interpreted by the fact that the former device displays more efficient charge extraction. *N* can be generated by integrating *C* with respect to the photovoltage. The device with TMAH treatments displays lower *N* than one without TMAH treatments, indicating enhanced charge extraction in the device with TMAH treatment. This consequence confirms that nanostructured UMG silicon substrates treated with TMAH are more suitable for hybrid organic−inorganic solar cells with efficient charge extraction, leading to a high performance.

Although the high-quality p−n junction fabricated by a thermal diffusion process is widely applied in solar cell engineering, the high-temperature method may not be appropriate for our surface upgraded

nanostructured UMG silicon substrate. Usually thermal diffusion p–n junction fabrication requires a high-temperature process (800–1000 °C).[5] At this high temperature, metal ion impurities in UMG silicon can diffuse randomly. In order to verify this assumption, the UMG silicon substrate is annealed at 1000 °C for 10 min under Ar ambience to simulate the high-temperature thermal diffusion fabrication process. The J–V curve of the device based on annealed nanostructured UMG silicon is plotted in Figure S5. The device gives a rather poor V_{OC} of 0.31 V and an inferior FF (0.50), yielding a PCE of only 3.78%. The poor V_{OC} and FF indicate serious recombination at the organic–inorganic interface. It reveals that the quality of the UMG silicon junction is degraded after the high-temperature annealing process.[37]

CONCLUSIONS

In conclusion, we have developed a low-temperature solution-processed processing method to fabricate efficient solar cells using UMG silicon. The MACE process partly upgrades the silicon quality and suppresses the SRH recombination at the surface, while accompanied nanostructured silicon can improve the light harvesting. The nanostructured silicon can allow using a thin substrate for a high-performance device, which relaxes the low-impurity requirement. The subsequent TMAH etching process reduces the surface recombination *via* controlling the surface area. A low-temperature organic–inorganic hybrid junction takes advantage of the simultaneous upgrading surface quality. A record PCE of 12.0% is achieved based on the UMG silicon/PEDOT:PSS heterojunction device, which combines the well-controlled surface morphology and low-temperature junction fabrication process. Our report opens a path for utilization of UMG silicon for high-performance solar cells, which can potentially reduce solar cell costs by using low-quality silicon.

EXPERIMENTAL SECTION

Thin UMG Silicon Substrate Fabrication. The thin UMG silicon substrate was etched from an n-type (100) Si wafer (0.9–13 Ω·cm, ~150 μm thickness). The substrate was submerged in KOH solution, and the concentration was about 50 wt % at ~90 °C for various times to acquire different thicknesses.

Nanostructured UMG Silicon Fabrication. The nanostructured silicon was fabricated by immersing the silicon substrate into an aqueous solution of HF (4.8 M) + $AgNO_3$ (0.02 M) at room temperature. Then the substrate was dipped into a HNO_3 and HF solution to eliminate any residual silver and silicon oxide, respectively. The nanostructured UMG silicon was then etched in 1 vol % TMAH solution for various times at room temperature in order to reduce the surface area.

Device Fabrication and Characterization. PEDOT:PSS (CLEVIOS PH 1000, with 1 wt % Triton and 5 wt % dimethyl sulfoxide (DMSO)) film was fabricated by a spin-casting process on silicon with a speed of 9000 rpm for 1 min. The substrate was annealed at 125 °C at ambient atmosphere. Finally, 200 nm thick silver top grid contacts and a 200 nm thick Al back contact were deposited by thermal evaporation (NANO 36, Kurt J. Lesker). The deposition of silver top grid contacts is carried out by thermal evaporation under 10^{-6} Torr. The metal covering part consists of 10% of the whole area of the top surface.

The current density–voltage characteristics were acquired by a Newport 91160 solar simulator to generate a simulated air mass (AM) 1.5 solar spectrum irradiation source at 100 mW/cm^2, which was calibrated by a Newport standard silicon solar cell 91150. The external quantum efficiency measurements were measured by a Newport monochromator 74125 and power meter 1918. The morphology of nanostructured UMG silicon was determined by an FEI Quanta 200 FEG high-resolution scanning electron microscope and an FEI Tecnai G2 F20 STWIN transmission electron microscope. The transient photovoltage measurements were measured over a range of white light intensities, where a green laser light source from an LED (532 nm, 30–200 mW, Kingbright) triggered by a functional signal generator was used to provide square-wave-modulated illumination, resulting in a small (10 mV) perturbation voltage; the photovoltage wave signals were recorded on a Tektronix oscilloscope. The transient photocurrent was consequently carried out with an impedance of 50 Ω. The impurities were detected by ICP-MS (Xeries II, Thermo Electron). The minority carrier lifetime was measured by microwave photoconductivity decay (WT-2000mPCD, Semilab).

Conflict of Interest: The authors declare no competing financial interest.

Acknowledgment. This work was supported by the National Basic Research Program of China (973 Program) (2012CB932402), the National Natural Science Foundation of China (91123005, 61176057, 61211130358), the Priority Academic Program Development of Jiangsu Higher Education Institutions, Jiangsu Key Laboratory for Carbon-Based Functional Materials and Devices, and Collaborative Innovation Center of Suzhou Nano Science and Technology. The authors thank Mr. Feng Bao for SEM characterization.

Supporting Information Available: Methods for calculating the capacitance and charge carrier concentration. Additional figures of cross-section SEM images of the different thicknesses of planar UMG silicon, transmission spectra of the planar UMG silicon with various thicknesses, I–V curve and EQE spectra of the devices based on PEDOT:PSS and planar UMG silicon with various thicknesses, cross-section SEM images of the nanostructured UMG silicon without and with TMAH treatment, cross-section SEM images of TMAH-modified nanostructured UMG silicon coated with PEDOT:PSS, cross-section image of nanostructured SG silicon, absorption and reflection spectra of the nanostructured UMG silicon with different surface structures, J–V curves of the device based on PEDOT:PSS and postannealed nanostructured UMG silicon, and tables of the photovoltaic performance of the devices based on PEDOT:PSS and planar UMG silicon with different thicknesses. This material is available free of charge *via* the Internet at http://pubs.acs.org.

REFERENCES AND NOTES

1. Pizzini, S.; Acciarri, M.; Binetti, S. From Electronic Grade to Solar Grade Silicon: Chances and Challenges in Photovoltaics. *Phys. Status Solidi A* **2005**, *202*, 2928–2942.
2. Woditsch, P.; Koch, W. Solar Grade Silicon Feedstock Supply for PV Industry. *Sol. Ener. Mater. Sol. Cells* **2002**, *72*, 11–26.
3. Yuge, N.; Abe, M.; Hanazawa, K.; Baba, H.; Nakamura, N.; Kato, Y.; Sakaguchi, Y.; Hiwasa, S.; Aratani, F. Purification of Metallurgical-Grade Silicon up to Solar Grade. *Prog. Photovolt: Res. Appl.* **2001**, *9*, 203–209.
4. Goodrich, A. C.; Powell, D. M.; James, T. L.; Woodhouse, M.; Buonassisi, T. Assessing the Drivers of Regional Trends in

Solar Photovoltaic Manufacturing. *Energy Environ. Sci.* **2013**, *6*, 2811–2821.
5. Zhao, J.; Wang, A.; Green, M. A.; Ferrazza, F. 19.8% Efficient "Honeycomb" Textured Multicrystalline and 24.4% Monocrystalline Silicon Solar Cells. *Appl. Phys. Lett.* **1998**, *73*, 1991.
6. Del Canizo, C.; Del Coso, G.; Sinke, W. Crystalline Silicon Solar Module Technology: Towards the 1 per Watt-Peak Goal. *Prog. Photovolt: Res. Appl.* **2009**, *17*, 199–209.
7. Khattak, C. P.; Joyce, D. B.; Schmid, F. A Simple Process to Remove Boron from Metallurgical Grade Silicon. *Sol. Ener. Mater. Sol. Cells* **2002**, *74*, 77–89.
8. Kwon, J. Y.; Lee, D. H.; Chitambar, M.; Maldonado, S.; Tuteja, A.; Boukai, A. High Efficiency Thin Upgraded Metallurgical-Grade Silicon Solar Cells on Flexible Substrates. *Nano Lett.* **2012**, *12*, 5143–5147.
9. Lee, D. H.; Kwon, J. Y.; Maldonado, S.; Tuteja, A.; Boukai, A. Extreme Light Absorption by Multiple Plasmonic Layers on Upgraded Metallurgical Grade Silicon Solar Cells. *Nano Lett.* **2014**, *14*, 1961–1967.
10. Shuttle, C. G.; O'Regan, B.; Ballantyne, A. M.; Nelson, J.; Bradley, D. D. C.; de Mello, J.; Durrant, J. R. Experimental Determination of the Rate Law for Charge Carrier Decay in A Polythiophene: Fullerene Solar Cell. *Appl. Phys. Lett.* **2008**, *92*, 093311.
11. Kayes, B. M.; Atwater, H. A.; Lewis, N. S. Comparison of the Device Physics Principles of Planar and Radial PN Junction Nanorod Solar Cells. *J. Appl. Phys.* **2005**, *97*, 114302.
12. Li, X.; Xiao, Y.; Bang, J. H.; Lausch, D.; Meyer, S.; Miclea, P.; Jung, J.; Schweizer, S. L.; Lee, J.; Wehrspohn, R. B. Upgraded Silicon Nanowires by Metal-Assisted Etching of Metallurgical Silicon: A New Route to Nanostructured Solar-Grade Silicon. *Adv. Mater.* **2013**, *25*, 3187–3191.
13. Coletti, G.; Bronsveld, P. C.; Hahn, G.; Warta, W.; Macdonald, D.; Ceccaroli, B.; Wambach, K.; Le Quang, N.; Fernandez, J. M. Impact of Metal Contamination in Silicon Solar Cells. *Adv. Funct. Mater.* **2011**, *21*, 879–890.
14. Sze, S. M. *Semiconductor Devices: Physics and Technology*; Wiley: New York, 2008.
15. Wang, S.; Weil, B. D.; Li, Y.; Wang, K. X.; Garnett, E.; Fan, S.; Cui, Y. Large-Area Free-Standing Ultrathin Single-Crystal Silicon as Processable Materials. *Nano Lett.* **2013**, *13*, 4393–4398.
16. Peng, K. Q.; Xu, Y.; Wu, Y.; Yan, Y.; Lee, S.; Zhu, J. Aligned Single-Crystalline Si Nanowire Arrays for Photovoltaic Applications. *Small* **2005**, *1*, 1062–1067.
17. Oh, J.; Yuan, H.; M. Branz, H. An 18.2%-Efficient Black-Silicon Solar Cell Achieved through Control of Carrier Recombination in Nanostructures. *Nat. Nanotechnol.* **2012**, *7*, 743–748.
18. Peng, K.; Wu, Y.; Fang, H.; Zhong, X.; Xu, Y.; Zhu, J. Uniform, Axial-Orientation Alignment of One-Dimensional Single-Crystal Silicon Nanostructure Arrays. *Angew. Chem. Int. Ed.* **2005**, *44*, 2737–2742.
19. Ma, X.; Zhang, J.; Wang, T.; Li, T. Hydrometallurgical Purification of Metallurgical Grade Silicon. *Rare Met. (Beijing, China)* **2009**, *28*, 221–225.
20. Zhong, X.; Qu, Y.; Lin, Y. C.; Liao, L.; Duan, X. Unveiling the Formation Pathway of Single Crystalline Porous Silicon Nanowires. *ACS Appl. Mater. Interfaces* **2011**, *3*, 261–270.
21. Li, S.; WenhuiMa; Zhou, Y.; XiuhuaChen; Xiao, Y.; Ma, M.; WenjieZhu; Wei, F. Fabrication of Porous Silicon Nanowires by MACE Method in $HF/H_2O_2/AgNO_3$ System at Room Temperature. *Nanoscale Res. Lett.* **2014**, *9*, 196–203.
22. Li, X.; Xiao, Y.; Yan, C.; Zhou, K.; Miclea, P.; Meyer, S.; Schweizer, S. L.; Sprafke, A.; Lee, J.; Wehrspohn, R. B. Self-Purification Model for Metal-Assisted Chemical Etching of Metallurgical Silicon. *Electrochim. Acta* **2014**, *138*, 476–480.
23. Sailor, M. J.; Ginsburg, E. J.; Gorman, C. B.; Kumar, A.; Grubbs, R. H.; Lewis, N. S. Thin Films of n-Si/Poly-$(CH_3)_3$-Si-Cyclooctatetraene: Conducting-Polymer Solar Cells and Layered Structures. *Science* **1990**, *249*, 1146–1149.
24. Shiu, S.; Chao, J.; Hung, S.; Yeh, C.; Lin, C. Morphology Dependence of Silicon Nanowire/Poly(3,4-ethylenedioxythiophene):Poly(styrenesulfonate) Heterojunction Solar Cells. *Chem. Mater.* **2010**, *22*, 3108–3113.
25. Avasthi, S.; Lee, S.; Loo, Y. L.; Sturm, J. C. Role of Majority and Minority Carrier Barriers Silicon/Organic Hybrid Heterojunction Solar Cells. *Adv. Mater.* **2011**, *23*, 5762–5766.
26. Shen, X.; Sun, B.; Liu, D.; Lee, S. Hybrid Heterojunction Solar Cell Based on Organic-Inorganic Silicon Nanowire Array Architecture. *J. Am. Chem. Soc.* **2011**, *133*, 19408–19415.
27. Zhang, F.; Sun, B.; Song, T.; Zhu, X.; Lee, S. Air Stable, Efficient Hybrid Photovoltaic Devices Based on Poly(3-hexylthiophene) and Silicon Nanostructures. *Chem. Mater.* **2011**, *23*, 2084–2090.
28. Chen, T. G.; Huang, B. Y.; Liu, H. W.; Huang, Y. Y.; Pan, H. T.; Meng, H. F.; Yu, P. Flexible Silver Nanowire Meshes for High-Efficiency Microtextured Organic-Silicon Hybrid Photovoltaics. *ACS Appl. Mater. Interfaces* **2012**, *4*, 6857–6864.
29. Chen, T.; Huang, B.; Chen, E.; Yu, P.; Meng, H. Micro-Textured Conductive Polymer/Silicon Heterojunction Photovoltaic Devices with High Efficiency. *Appl. Phys. Lett.* **2012**, *101*, 033301.
30. Liu, Q.; Ono, M.; Tang, Z.; Ishikawa, R.; Ueno, K.; Shirai, H. Highly Efficient Crystalline Silicon/Zonyl Fluorosurfactant-Treated Organic Heterojunction Solar Cells. *Appl. Phys. Lett.* **2012**, *100*, 183901.
31. Jeong, S.; McGehee, M. D.; Cui, Y. All-Back-Contact Ultra-Thin Silicon Nanocone Solar Cells with 13.7% Power Conversion Efficiency. *Nat. Commun.* **2013**, *4*, 2950–2956.
32. Pietsch, M.; Bashouti, M. Y.; Christiansen, S. The Role of Hole Transport in Hybrid Inorganic/Organic Silicon/Poly(3,4-ethylenedioxy-thiophene):Poly(styrenesulfonate) Heterojunction Solar Cells. *J. Phys. Chem. C* **2013**, *117*, 9049–9055.
33. Wei, W. R.; Tsai, M. L.; Ho, S. T.; Tai, S. H.; Ho, C. R.; Tsai, S. H.; Liu, C. W.; Chung, R. J.; He, J. H. Above-11%-Efficiency Organic-Inorganic Hybrid Solar Cells with Omnidirectional Harvesting Characteristics by Employing Hierarchical Photon-Trapping Structures. *Nano Lett.* **2013**, *13*, 3658–3663.
34. Erickson, A. S.; Zohar, A.; Cahen, D. n-Si-Organic Inversion Layer Interfaces: A Low Temperature Deposition Method for Forming a p-n Homojunction in n-Si. *Adv. Energy Mater.* **2014**, *4*, DOI: 10.1002/ aenm.201301724.
35. Yu, P.; Tsai, C.; Chang, J.; Lai, C.; Chen, P.; Lai, Y.; Tsai, P.; Li, M.; Pan, H.; Huang, Y.; *et al.* 13% Efficiency Hybrid Organic/Silicon Nanowire Heterojunction Solar Cell *via* Interface Engineering. *ACS Nano* **2013**, *7*, 10780–10787.
36. Price, M. J.; Foley, J. M.; May, R. A.; Maldonado, S. Comparison of Majority Carrier Charge Transfer Velocities at Si/Polymer and Si/Metal Photovoltaic Heterojunctions. *Appl. Phys. Lett.* **2010**, *97*, 083503.
37. Kim, J.; Yoon, S. Y.; Choi, K. Effects of Phosphorus Diffusion Gettering on Minority Carrier Lifetimes of Single-Crystalline, Multi-Crystalline and UMG Silicon Wafer. *Curr. Appl. Phys.* **2013**, *13*, 2103–2108.
38. Yella, A.; Lee, H. W.; Tsao, H. N.; Yi, C.; Chandiran, A. K.; Nazeeruddin, M. K.; Diau, E. W. G.; Yeh, C. Y.; Zakeeruddin, S. M.; Gratzel, M. Porphyrin-Sensitized Solar Cells with Cobalt (II/III)-Based Redox Electrolyte Exceed 12% Efficiency. *Science* **2011**, *334*, 629–634.
39. Ehrler, B.; Musselman, K. P.; Böhm, M. L.; Morgenstern, F. S.; Vaynzof, Y.; Walker, B. J.; MacManus-Driscoll, J. L.; Greenham, N. C.; Musselman, K. P.; Böhm, M. L.; *et al.* Preventing Interfacial Recombination in Colloidal Quantum Dot Solar Cells by Doping the Metal Oxide. *ACS Nano* **2013**, *7*, 4210–4220.